SENSITIVITY OF LONG-TERM BARE-SOIL INFILTRATION SIMULATIONS AT YUCCA MOUNTAIN, NV

Stuart A. Stothoff
Center for Nuclear Waste Regulatory Analyses
Southwest Research Institute
San Antonio, TX 78238-5166, USA

ABSTRACT

Numerical modeling of long-term infiltration into the deep subsurface while including the effects of climatic variation poses a significant computational challenge. This challenge is, in part, related to the fact that moisture levels in the top several meters of a porous matrix are strongly affected by atmospheric conditions over time scales on the order of a decade. From theoretical considerations, a persistent underprediction of infiltration is expected to result from using time-averaged weather for boundary conditions. In order to examine the time-averaging effects on infiltration, a hypothetical porous medium sensitive to atmospheric conditions is considered. By comparing bare-soil simulations using hourly values of weather inputs with simulations using various types of averaging for the weather inputs, it is demonstrated that straightforward averaging of the weather does indeed underpredict infiltration. It is further demonstrated that capturing the full variability of the weather within an event window of a day or two around rainfall events, while using monthly or longer averages outside the window, is sufficient to accurately capture the infiltration behavior. Precipitation is the most critical parameter to capture; atmospheric vapor density is the next most critical parameter. The importance of accounting for weather variability increases with both the permeability of the porous medium and the atmospheric relative humidity. For porous media representative of Yucca Mountain soil columns and hourly weather representative of the Yucca Mountain area, a one-day event window is quite accurate. When considering infiltration into alluvium, it is found that as capillary effects become stronger net infiltration decreases, while surprisingly, as permeability increases net infiltration decreases.

INTRODUCTION

Recent total-system performance assessments of the proposed geologic repository for high-level nuclear waste at Yucca Mountain, NV, generally agree that the calculation of cumulative releases to the accessible environment over 10,000 years is highly sensitive to the deep percolation rate, or net liquid flux through the repository (Nuclear Regulatory Commission, 1992, 1994; Sandia National Laboratories, 1992, 1994; Electric Power Research Institute, 1990, 1992). In all of these performance assessments, however, the magnitudes and distributions of infiltration rates used in the calculations have largely been based on assumptions and heuristic arguments. Moreover, these infiltration rates assume both spatial and temporally averaged values. This numerical modeling study was motivated by the need to provide physically based estimates of infiltration rates for Yucca Mountain, to understand the impact of averaging, and to determine the meteorologic parameters that most significantly influence the calculation of net infiltration. This information, in turn, is intended to be utilized in detailed analyses of deep percolation.

In order to provide a more realistic approximation for deep percolation, one avenue being considered is numerically simulating the water balance across the air-soil interface in order to provide boundary conditions for simulations of deeper flows. Due to the very long time frame for high-level waste simulations, computational efficiency in such near-surface simulators is of practical importance. The purposes of this modeling study are two-fold: (i) present the mathematical theory of a model designed to simulate coupled flow of moisture and energy in a partially saturated porous medium, and (ii) illustrate the use of the model by addressing two questions about infiltration at Yucca Mountain. What detail in weather information is required to accurately simulate infiltration? What is the range of infiltration rates that might be expected through surficial deposits? For simplicity, the current work neglects the effect of fast pathways (e.g., fractures) and vegetation, both of which are expected to have potentially strong influences on net infiltration. As net infiltration is expected to be highest in areas with relatively permeable surface media, this work primarily considers the behavior of alluvium.

From the standpoint of computational efficiency, averaging the weather inputs (e.g., precipitation, solar radiation, air temperature) can provide significant speedups, at the cost of a loss in accuracy. The minimum desirable averaging period is one day, with a week or longer highly desirable. Synthetic daily or seasonal weather inputs are easier to generate than shorter-term weather, and weather boundary condition files input to simulators are much more compact. Averaging weather inputs over a day or several days has the advantage of removing the computational burden of the diurnal cycle, which, in the arid environment under consideration, can impose a large swing in temperature over the course of a day and impose dozens to hundreds of time steps per day to accurately resolve. With averaging over a week, allowing a weekly time step, a simulation can proceed much faster. However, due to the nonlinear behavior of the hydraulic parameters relevant to moisture flow in porous media, it may be suspected that smearing the boundary conditions in time may lead to quite erroneous predictions of infiltration, particularly when evaporation is under climate control. In some preliminary simulations, it was found that infiltration predictions were dominated by alarmingly large time-averaging errors, prompting this study; as data characterizing Yucca Mountain become available, the time-averaging errors have decreased.

Near-surface moisture redistribution can be characterized by a series of event pairs, consisting of an infiltration event followed by an evaporation event (Black et al., 1969; Gardner, 1973; Gardner, 1974; Eagleson, 1978; Clapp, 1982; Milly, 1986). The success of event-based approaches arises from the tendency for evaporation to proceed at two limiting rates, depending on the available moisture at the ground surface. When the soil is moist, evaporation rates are climate controlled. After the ground surface dries out, evaporation rates are soil controlled, or determined by the ability of the soil to provide vapor. A straightforward method for handling time averaging, explicitly taking into account the precipitation and evaporation events, is shown to be quite accurate.

NUMERICAL SIMULATOR

A one-dimensional (1D) finite element model of coupled moisture and energy transport in a porous medium, BREATH (Stothoff, 1995), was used to simulate the response of the near-surface soil profile. The simulator couples the Richards equation with diffusive vapor transport, assuming local equilibrium between vapor and liquid. The energy transport model considers diffusive flux in the matrix as well as advective transport via liquid and vapor fluxes. Equation development and various test examples are presented in the user documentation (Stothoff, 1995); the governing equations are summarized here for completeness. The model is one-dimensional, but notation is in vector form for conciseness.

The simulator solves the moisture mass balance equation.

$$\frac{\partial}{\partial t}(\theta_w \rho_w + \theta_g \rho_v) + \nabla \cdot (\rho_w \mathbf{q}_w + \rho_v \mathbf{q}_v) = 0. \tag{1}$$

where θ_w and θ_g are the liquid water and the gas phase volumetric fractions. ρ_w and ρ_v are the liquid water and vapor densities, and $\mathbf{q}_w$ and $\mathbf{q}_v$ are the liquid water and vapor fluxes. The moisture balance equation is subject to the following constraints and constitutive assumptions:

$$\theta_w + \theta_g = \varepsilon, \tag{2}$$

$$\mathbf{q}_w = -K_{sat} k_{rel} (\nabla \psi + \nabla z), \tag{3}$$

$$\rho_v \mathbf{q}_v = -D\theta_g \nabla \rho_v, \tag{4}$$

$$\rho_v = \rho_{vs} \exp(\psi g / R_v T), \tag{5}$$

$$\rho_{vs} = \exp[46.44 - (6.028/T) - 6790 \ln(T)], \tag{6}$$

where ε is porosity, K_{sat} is the saturated hydraulic conductivity, k_{rel} is the relative permeability, ψ is matric potential, z is the elevation above a datum, D is the vapor diffusion coefficient (including a constant tortuosity), g is the gravitational constant, T is the temperature in °K, R_v is the gas constant for vapor, and ρ_{vs} is the saturated vapor density in gm/cm^3.

A modification of the van Genuchten (1980) relationships is used,

$$k_{rel}(\psi) = \begin{cases} [1 - \beta^{n-1}(1+\beta^n)^{-m}]^2 (1+\beta^n)^{-m/2} & \text{if } \psi < \psi_0, \\ 1 & \text{if } \psi \geq \psi_0, \end{cases} \tag{7}$$

$$\theta_w(\psi) = \begin{cases} \theta_{wr} + (\theta_{ws} - \theta_{wr})[1+\beta^n]^{-m} & \text{if } \psi < \psi_0, \\ \theta_{wr} + (\theta_{ws} - \theta_{wr})[1+\beta_0^n]^{-m} + S_s(\psi - \psi_0) & \text{if } \psi \geq \psi_0, \end{cases} \tag{8}$$

$$m = 1 - (1/n), \tag{9}$$

$$\beta = \alpha|\psi| \quad \text{with } \beta_0 = \beta(\psi_0), \tag{10}$$

where α is related to the pore entry pressure, m is a scaling parameter, and S_s is the saturated specific storage coefficient. Equation 7 is based on the relative permeability relationship proposed by van Genuchten (1980) using the theory of Mualem (1976). Equation 8 is the extension to the van Genuchten (1980) moisture retention relationship proposed by Paniconi et al. (1991); continuity requirements are imposed such that $\psi = \psi_0$ where $S_s = \mathrm{d}\theta_w/\mathrm{d}\psi$. Hysteresis is neglected in both the moisture retention and mobility relationships.

The simulator also solves an energy balance equation, in the form

$$\frac{\partial}{\partial t}[(\theta_s \rho_s C_{Vs} + \theta_w \rho_w C_{Vw} + \theta_g \rho_v C_{Vv})\Phi + \theta_g \rho_v H_{lv}] + \nabla \cdot [\rho_w \mathbf{q}_w C_{Pw} + \rho_v \mathbf{q}_v (C_{Pv} + H_{lv}) - K_e \nabla \Phi] = 0, \tag{11}$$

where C_{Vv}, C_{Vw}, and C_{Vs} are the heat capacities at constant volume for vapor, liquid water, and the solid matrix. C_{Pv} and C_{Pw} are the heat capacities at constant pressure for vapor and liquid water. H_{lv} is the coefficient of latent heat for vapor. K_e is the thermal conductivity of the soil, and $\Phi = T - T_0$ is the temperature difference from reference state T_0.

The energy balance equation uses a simple weighted average thermal conductance,

$$K_e = \theta_w \rho_w k_e^w + \theta_s \rho_s k_e^s, \tag{12}$$

where k_e^w and k_e^s are the liquid and solid thermal conductances and the contribution of the air phase is neglected.

Neither thermally driven liquid flow nor thermal effects on transport coefficients are considered in this paper. Milly (1984a, 1984b) considered thermal effects on evaporation and concluded that neglecting liquid flow due to thermal forcings leads to errors on the order of 1 percent for long-term predictions, although there may be differences between simulated and measured near-surface moisture contents at a diurnal time scale. Neglecting thermal effects on transport coefficients (i.e., viscosity variation) was found to yield errors no more than 5 percent.

The ground surface is considered a flux boundary for liquid and a mixed-type boundary for vapor and energy. Liquid fluxes are assumed to be zero unless precipitation occurs. Precipitation is applied as a flux condition unless the surface reaches saturation, whereupon the top boundary condition switches to an incipient ponding (specified moisture content) condition, and any excess flux is assumed to run off. A diffusive vapor flux condition is assumed to hold whenever the surface layer is unsaturated, with

$$\mathbf{q}_v = k_v(\rho_{va} - \rho_v), \tag{13}$$

where k_v is a vapor conductance and ρ_{va} is the vapor density in the atmosphere. The energy boundary condition accounts for the energy advected past the boundary through liquid and vapor transport, as well as sensible heat transport and longwave and shortwave radiation, in the form

$$\mathbf{q}_e = \rho_w \mathbf{q}_w C_{Pw} + \rho_v \mathbf{q}_v (C_{Pv} + H_{lv}) + k_h(T_a - T) + (1 - \alpha_s)S_t + \sigma(\epsilon_a T_a^4 - \epsilon_s T^4), \tag{14}$$

where k_h is a sensible heat conductance, T_a is the atmospheric temperature, α_s is albedo, S_t is shortwave radiation, σ is the Stefan-Boltzmann constant, ϵ_a is the atmospheric emissivity, and ϵ_s is the surface emissivity. Further discussion of the surface boundary conditions is found in the Appendix.

The bottom boundary is represented by a zero-gradient condition for moisture content, vapor density, and temperature. The zero-gradient moisture content condition implicitly assumes that there must be liquid flux moving out from the bottom through gravity drainage whenever the moisture content is greater than the residual moisture content. Energy is advected out the bottom with the gravity drainage.

The energy balance and the moisture balance equations are solved sequentially. Each time step, the solution procedure cycles between the energy and the moisture balance equations, updating temperature- and head-dependent parameters. Within a cycle, each equation is iterated to convergence: a stricter convergence criterion is used each cycle. Time steps are adaptively adjusted to maintain a target of roughly nine moisture-equation iterations per time step. The moisture balance equation is solved using the mixed-form modified Picard finite element procedure of Celia et al. (1990), extending the approach to incorporate vapor transport. The energy balance equation is solved using standard finite element methods. Both balance equations are solved using piecewise-linear basis functions for the spatial terms and lumped time terms.

THEORETICAL CONSIDERATIONS

A convenient qualitative framework for examining long-term infiltration was presented by Salvucci (1994), based on work by Eagleson in the late 1970s, in which the long-term response of a 1D soil profile to atmospheric forcing was obtained by numerical simulation. Evaporation rates were based on mean yearly atmospheric conditions; however, individual precipitation events were stochastically generated. Attempting to find the mean infiltration flux, Salvucci (1994) analytically

and numerically demonstrates that, for an isothermal Brooks-Corey soil, short-term variations of moisture content around the equivalent steady-state profile lead to an infiltration flux greater than the flux predicted from the equivalent steady-state moisture profile. Still considering an isothermal soil, but generalizing the Salvucci (1994) results slightly, consider the Buckingham-Darcy flux law

$$\mathbf{q}_w = -K_{sat} k_{rel} (\nabla \psi + \nabla z). \tag{15}$$

Denoting θ_w by θ, expressing θ and $\mathbf{q}_w$ in terms of a temporal mean $\overline{(\bullet)}$ and a perturbation $(\bullet)'$, and performing a first-order expansion about the temporal mean moisture content, yields

$$\overline{\mathbf{q}_w} + \mathbf{q}_w{}' = -K_{sat} \left(\overline{k_{rel}} + \left. \frac{\mathrm{d}k_{rel}}{\mathrm{d}\theta} \right|_{\overline{\theta}} \theta' \right) \left[\nabla \overline{\psi} + \left. \frac{\mathrm{d}\psi}{\mathrm{d}\theta} \right|_{\overline{\theta}} \nabla \theta' + \nabla z \right]. \tag{16}$$

Rearranging, the expected mean temporal flux is

$$< \mathbf{q}_w > = -K_{sat} \overline{k_{rel}} \left(\nabla \overline{\psi} + \nabla z \right) - \frac{K_{sat}}{2} \left. \frac{\mathrm{d}k_{rel}}{\mathrm{d}\theta} \right|_{\overline{\theta}} \left. \frac{\mathrm{d}\psi}{\mathrm{d}\theta} \right|_{\overline{\theta}} < \nabla (\theta')^2 >, \tag{17}$$

denoting an expected value by $< (\bullet) >$. The last term on the right-hand side comes from the temporal average of the product of two perturbations, and only occurs due to the dependence of the relative permeability on moisture content. Salvucci (1994) compares the coupling of the mean and perturbation equations to the "closure" problem in turbulence.

A number of implications stem from this simple first-order theory. First, assuming that all perturbations in moisture content result from atmospheric forcing, the expected value of the squared perturbation decays with depth; noting that both $\mathrm{d}k_{rel}/\mathrm{d}\theta$ and $\mathrm{d}\psi/\mathrm{d}\theta$ are positive, there is a flux of liquid from the surface into the soil greater than that predicted by the long-term average moisture content profile. Second, the long-term average moisture content will never be greater than the equivalent steady-state moisture content calculated using the long-term average moisture flux. Third, at a depth where the perturbations have decayed to zero, the moisture content profile is a good predictor of flux. Fourth, if the magnitude of the perturbation forcing diminishes, one would expect that the overall moisture profile would become drier and the deep infiltration flux would decrease. Fifth, application of gravity-drainage boundary conditions acts to dampen perturbations, thereby underpredicting the drainage flux, so that care must be used to ensure that gravity-drainage conditions are used only where a zone of gravity drainage exists above the boundary. Finally, as time-averaging decreases the magnitude of perturbations to the system, one would expect that time-averaging must yield a persistent bias to the computation, so that the system is too dry and deep infiltration is underpredicted.

Following a similar perturbation approach for the vapor flux, expressed by

$$\mathbf{q}_v = -D(\varepsilon - \theta) \nabla \rho_v, \tag{18}$$

and assuming that products of temperature perturbations with moisture content perturbations are zero and that D is constant, yields

$$< \mathbf{q}_v > = -D(\varepsilon - \overline{\theta}) \nabla \overline{\rho_v} + \frac{D}{2} \left. \frac{\mathrm{d}\rho_v}{\mathrm{d}\theta} \right|_{\overline{\theta}} < \nabla (\theta')^2 > . \tag{19}$$

The vapor flux has a coupling term with the opposite sign from that found with the liquid flux analysis: thus perturbations in moisture content (but not temperature) are expected to yield a net upward perturbation flux of vapor greater than that predicted by the mean profile. Milly (1984a, 1984b) found that nonisothermal vapor flux is less important than isothermal vapor flux

on long-term evaporation predictions, which is in agreement with the finding that temperature perturbations do not have an effect on expected vapor flux. A perturbation examination of the diffusive energy flux (by far the largest component of energy transfer in natural soils) does not yield a coupling term, implying that the mean temperature profile is a good predictor for the net diffusive flux of energy.

The first-order theory asserts that, regardless of issues of material heterogeneity and neglecting vapor flux, numerical simulators must underpredict long-term average moisture content and long-term average deep liquid flux when the boundary conditions are time averaged. As upward vapor flux must also be underpredicted, however, there may be compensating errors. The following sections examine the magnitude of the predicted errors under different time-averaging schemes.

INPUT DATA

Atmospheric forcings were based on a ten-year sequence, March 1984 through February 1994, of hourly weather readings from the National Weather Service at Desert Rock, Nevada. The Desert Rock station is at an elevation of 1000 m, while Yucca Mountain ranges in elevation from 1250 m to nearly 1800 m, thus the readings are presumably somewhat warmer and drier than would have been observed on Yucca Mountain proper. The readings include atmospheric temperature, relative humidity, wind speed, total cloud cover, and an hourly rainfall rate code. Shortwave and longwave radiation were estimated from the hourly values of cloud cover also available from the Desert Rock station. The calculated radiation values were not compared to field measurements, but should vary realistically with the other weather parameters so that the effects of time averaging are reasonable. Daily Desert Rock precipitation totals are also available; these were disaggregated into hourly values using the hourly rainfall rate code. The atmospheric variables available to the simulator on an hourly basis include precipitation, 2-m elevation atmospheric temperature, 2-m elevation atmospheric vapor density, incident longwave radiation, incident shortwave radiation, and 2-m elevation wind speed. The atmospheric data set has an average precipitation of 160 mm/yr, average temperature of 17 °C, average vapor density of 4.5×10^{-6} gm/cm^3, average incident longwave radiation of 320 W/m^2, average incident shortwave radiation of 250 W/m^2, and average wind speed of 4.1 m/s.

Time averaging was performed by taking a moving average of the input weather components, either singly or in groups. A moving average of a component is simply the average value of the component over a window centered on the current value, or

$$\overline{V_i} = \frac{\sum_{j=i-N}^{i+N} V_j}{2N+1}, \tag{20}$$

where V_i is a component being averaged and $2N+1$ is the window over which the component is being averaged. In order to ensure that each i value had a full moving-average window, the beginning and end of the time series were artificially extended with the first and last N values of the time series.

As will be demonstrated, using a moving average of the input data leads to inaccuracies. Reasoning that the moving average is most inaccurate when evaporation is climate-controlled leads to the idea of an event window, in which one or more averaged weather data inputs are replaced with the original hourly readings. The event window is tied to precipitation events. Two types of event windows will be considered, a symmetric window centered on each precipitation hour, and an unsymmetric window starting at each precipitation hour.

In examining the effects of time averaging, a synthetic porous medium was simulated. The synthetic media properties are representative of a welded tuff, except that K_{sat} is orders of magnitude larger than realistic welded tuffs and in the range of alluvium. The synthetic medium is

strongly affected by capillary properties: thus it can supply liquid from deeper within the column than actual alluvium, thereby maintaining wetter conditions at the surface and accentuating any time-averaging errors. The properties of all porous media considered in this study, including tuffs and alluvia representative of Yucca Mountain, are shown in Table 1. The tuff properties are taken from Flint and Flint (1994), while the ranges of alluvium properties considered are in the range reported by Guertal et al. (1994), Hudson et al. (1994), Hevesi and Flint (1993), and Hevesi et al. (1994). Residual moisture contents were not presented in the references: all residual moisture contents are here assumed to be zero.

In all of the presented simulations, a 30-m column was modeled, to ensure that the lower boundary conditions have a relatively small effect on the moisture and temperature profiles. Element lengths smoothly increase with depth. For the synthetic material, the top element is 2 cm; for the other media, the top element size ranges from 1 mm to 10 cm, with smaller top elements used for less permeable media.

RESULTS OF TIME AVERAGING

For the purposes of this study, the effects of time averaging are examined using the ten-year average of moisture content and the ten-year average moisture flux, where the moisture flux is the sum of the liquid and vapor fluxes. At the end of each time step, the average value is updated using the formula

$$\overline{V}|^{CUM} = \frac{(CUM - \Delta t)\overline{V}|^{CUM-\Delta t} + \Delta t V|^{CUM}}{CUM}, \tag{21}$$

where CUM is the cumulative time from the start of the simulation and Δt is the time step size. Long-term cumulative results of this type should be viewed with caution in the 20 to 50 cm closest to the ground surface, especially fluxes calculated for short averaging periods. Reliable results in this top zone require extremely tight convergence criteria to control numerical roundoff errors, as instantaneous fluxes during wetting events can be 4 or 5 orders of magnitude greater than the average fluxes. Below this zone, flux calculations are reasonably reliable. Overall, the global mass balance was very good: for a representative case, the no-averaging base case, the moisture mass balance is 0.08 percent and the energy balance is 0.9 percent, where the balance is calculated by dividing the absolute value of the balance discrepancy by the sum of the absolute values of the net boundary fluxes.

Each simulation is started with a uniform moisture content of 0.0247 throughout the column, which is the bottom moisture content obtained by repeating the ten-year weather for a few centuries of simulated time. The long-term average profile is much drier at the top than the bottom, so the initial profile should exhibit upward moisture flux as the excess moisture at the top of the column is evaporated. A negative flux indicates upward movement of moisture.

The first example of the effects of averaging is shown in Figure 1, in which all weather components are averaged. A representative set of window sizes is used, with $2N + 1 = 3$ hr, 7 hr, 13 hr, 1 dy, 1 wk, and 1 mo. The result of using no averaging is also shown for comparison (the raw hourly data case). In Figure 1a, the 10-yr average moisture content is shown for each window size; the comparable 10-yr average moisture flux, or sum of liquid and vapor fluxes, is shown in Figure 1b. Vapor fluxes are comparable to liquid fluxes in the top 20 cm, in the opposite direction, but are negligible below this depth.

In accordance with the qualitative predictions of the linearized theory, there is a clear trend towards a drier column as the length of the averaging window increases, until the moving average window is greater than a week in length. Perhaps more significant, as the averaging window

increases, the predicted net evaporative flux increases (the moisture flux becomes more negative), so that the predicted net upward flux for the fully averaged case is roughly 4 times greater than the predicted flux for the case with no averaging. Even the minimum desirable averaging length of one day overpredicts the net evaporative flux by more than 2-1/2 times. Clearly, averaging weather inputs can lead to gross errors in moisture flux predictions.

In Figure 2, the results from a series of averaging schemes is presented. In this figure, the vertical axis is $\max(|\mathbf{q}_{raw} - \mathbf{q}|)_{x>20\,\mathrm{cm}}$, or the absolute value of the maximum deviation of the moisture flux from the no-averaging base case below a depth of 20 cm. The horizontal axis represents various parameters, such as moving average length or event window size, which is different for each curve. As a reference, the curves shown in Figure 1 are represented as a single curve labeled MA, with the varying parameter being the total length of the moving average window in days.

Several other sensitivities are examined in Figure 2. As will be subsequently demonstrated, an accurate representation of precipitation events is the most important step in capturing the response of the soil-moisture profile to precipitation/evaporation dynamics, but is not sufficient by itself. Accordingly, the remaining simulations all capture precipitation with one-hour increments, the finest resolution data available. The effects of capturing evaporation accurately are examined by changing the size of the event window, within which all weather variables are resolved at a one-hour interval and outside of which a one-month average is used. In one sequence, labeled SEW, an event window is symmetrically placed about each precipitation event; in another, labeled AEW, an event window is asymmetrically placed, starting at a precipitation event. In these two cases, the parameter varied is the one-sided length of the event window in days. The event window is quite effective in reducing time-averaging inaccuracies, reducing discrepancies in fluxes by more than two orders of magnitude with only a two-day event window. Slightly greater accuracy is achieved by using a symmetric window instead of an asymmetric one, which might be attributed to recovering a diurnal temperature (and vapor density) profile at the precipitation event that is more representative of daily patterns.

Reasoning that small rainfall events should not affect deep infiltration, the effect of not using an event window for small rainfall events is shown in Figure 2, with the curve labelled TPL. A two-day symmetric event window is used for events that are above a threshold precipitation level (threshold statistics are shown in Table 2) and averaged weather is used below the threshold. Precipitation is accurately represented in all cases. The varying parameter in Figure 2 is the threshold rainfall event in tenths of an inch per hour. Interestingly, even relatively small (0.03 in/hr) rainfall events benefit from the use of an event window: the accuracy of a two-day symmetric event window simulation using a 0.03 in/hr rainfall threshold is equivalent to that of a half-day event window not using thresholds.

In order to verify the conclusion that an event window of only a day or two is necessary for reasonably accurate simulations, a synthetic data set representative of wetter and cooler conditions is applied to the soil column. The synthetic data set was derived from the original weather by subtracting 10 °C from each hourly temperature reading, multiplying the precipitation by 2, and multiplying the atmospheric vapor density by 2/3. The remaining atmospheric components were assumed to remain the same. These scaling parameters are based on six years of observations from the 3 Springs Creek station in central Nevada (McKinley and Oliver, 1994), which is at an elevation of 2,140 m. Note that, even though the vapor density is decreased, relative humidity is significantly higher due to the cooler temperatures.

The results from the simulations of the wetter and cooler environment are plotted as the curve labeled WC in Figure 2, where the varying parameter is the one-sided length of the event window in days. Again using an averaging period of one month and varying the event window shows that an event window of a few days captures almost all of the behavior of the non-averaged base case.

As opposed to the previously presented cases, there is a large net influx of water to the column, instead of a slight efflux. In this example, the influx with all weather components averaged is about half that of the case with no averaging. Although the percentage change is smaller than in the first example, the magnitude of the difference is larger. In this wetter and cooler environment, each event window size is less effective than in the base case. Nevertheless, the two-day event window again performs quite respectably. The size of the appropriate event window is shown to be somewhat site specific.

Further experimentation, not shown here, indicates that once an appropriate event window is selected, simulations are relatively insensitive to the length of the moving average even to six months or a year. This is reasonable from the standpoint that, once evaporation becomes soil-controlled, the main effect the atmosphere has on the soil column is on the soil temperature profile. Vapor transport is affected by temperature gradients, but is negligible below 20 cm, thus capturing the temperature profile in detail is not necessary.

The effects of the remaining atmospheric components are examined by one-month averaging all nonprecipitation weather variables within the event window except for the selected component, which uses its hourly values. The atmospheric components considered are vapor density (V), wind speed (W), air temperature (T), shortwave radiation (S), and longwave radiation (L). For comparison, the one-month average case (1mo), a case using one-month averaging only for rain (A), and a case using one-month averaging for all atmospheric components except rain (R) are shown as well. A two-day symmetric precipitation event window is used in each case. As shown in Figure 3, atmospheric vapor density is by far the most important variable to capture within an event window. This can be explained by noting that atmospheric vapor density during and after storms is usually much higher than the long-term average, thus evaporation is considerably over-predicted using the long-term average; other variables are not generally affected by storms to anywhere near the same extent. By comparing the error in the V curve at the surface with the symmetric event window curve in Figure 2, however, it can be seen that the error with accurately capturing only atmospheric vapor density in the event window is still nearly two orders of magnitude greater than the error remaining when all weather variables are accurately captured simultaneously.

Finally, in order to assess the importance of weather averaging for different porous media available at Yucca Mountain, several representative media were subjected to the raw hourly weather and one-month averaged weather with the original hourly rainfall. Parameters for the media are shown in Table 1. The deviation between the two predictions is shown in Figure 4. These simulations indicate that both the magnitude of the deviation and the deviation penetration depth decrease as the intrinsic permeability decreases, as might be expected.

ALLUVIUM PARAMETER SENSITIVITY

Yucca Mountain is characterized by a series of ridges and washes. Due to the steep wash slopes, it is anticipated that overland flow will find its way to the wash bottoms, filled with less than 20 m of potentially transmissive alluvium in most places. Therefore, it is of interest to determine what types of recharges might be expected through the alluvium layer. The following is an attempt to assess recharge sensitivities strictly due to alluvium properties. No attempt is made to accommodate vegetation, layering, fast flow pathways, or deviations from the Desert Rock weather, although these factors will undoubtedly be quite important in characterizing actual recharges.

As with the time-averaging study, a 30-m column is selected; however, the simulations are run, repeating the weather data, until the value of a constant cumulative moisture flux throughout the soil column can be determined. Based on the results from the time-averaging study, a one-month moving average with a symmetric one-day event window was considered accurate enough to characterize the weather. In general, once the ten-year-average moisture flux is constant throughout

the column, the column has reached a ten-year cyclic steady state, where the moisture and temperature profiles repeat every ten years. For the parameters considered here, cyclic steady state takes decades to centuries to achieve.

In this sensitivity analysis, it is assumed that the soil is characterized by van Genuchten (1980) parameterization. In all cases, porosity is 0.3 and residual moisture content is assumed to be zero. The effect of varying the three factors characterizing soil resistance to liquid flow (K_{sat}, α, and m) is examined by picking selected values of the parameters within the range appropriate for Yucca Mountain. The parameter values used, the average bottom moisture content, and the average flux exiting the bottom boundary are shown in Table 3.

For a given moisture content, increasing m yields a higher relative permeability and a lower capillary pressure. Similarly, increasing α yields a lower capillary pressure but does not affect the relative permeability. Increasing m and α corresponds to making the medium more uniform and coarser.

Three sets of parameter sensitivity checks are shown in Figure 5. The sensitivity of the response to α is shown using a low permeability and an average m value; as the air entry pressure increases (α decreases), both the long-term average moisture content and the long-term average flux decrease. Using the same base case but varying m, it is found that increasing m (making the soil more uniform) tends to dry the soil but allow greater fluxes through the column. Finally, by varying K_{sat} it is found that the long-term average moisture content decreases as K_{sat} increases: counterintuitively, the long-term average flux decreases dramatically as K_{sat} increases. Obviously, as K_{sat} decreases there is a limit to how much flux can be maintained; the limit is already being felt at lower K_{sat} in Figure 5, judging from the change in slope of the permeability curve. For the cases examined, the long-term average deep saturation ranged from 15 to 69 percent, while the average deep infiltration flux ranged from 0.026 to 19 percent of average annual precipitation. Using appropriate other combinations of the same parameters would yield even more extreme behavior.

The result that infiltration decreases as K_{sat} increases is quite surprising, as presumably wetting pulses would penetrate deeper in a more permeable material and thus be less susceptible to evaporation. The result is not unprecedented, as increasing evaporation has been linked to increasing K_{sat} in the presence of a water table (Czarnecki, 1990); however, in Czarnecki's work the water table provides a source of moisture at depth which is not present in the current simulations. Young and Nobel (1986) also found that increasing K_{sat} increases evaporation; however, no explanation is offered and the lower boundary condition is not presented. Vapor transport does not provide an explanation in the current study, as vapor fluxes are fairly constant across the various cases. It may be that the perturbative pumping action from precipitation events is more effective with a wetter medium; often a lower-permeability medium will be wetter than a corresponding high-permeability medium, as is the case here. Notably, the range of moisture contents is larger for the lower permeability media.

CONCLUSIONS

A number of conclusions can be drawn from this work. Based on theoretical arguments, and presuming that the flow system is adequately modeled, any numerical infiltration simulator must underpredict both the net downward liquid flux and the net upward vapor flux if any time-averaging in the weather inputs is present. Even though these errors are compensating, in the arid environments considered herein the error in net downward liquid flux appears to dominate the error in net upward vapor flux and net infiltration is underpredicted. The theoretical conclusion is supported by each of the numerical experiments reported, for both net drying and net wetting simulations; however, in a few experiments not shown here, when the initial conditions for the system were not

near an equilibrium state some portions of the simulated column did show slightly wetter conditions using averaged weather inputs than using the raw weather inputs. A characteristic of an equilibrium state is that cumulative fluxes are constant with depth, which is clearly not the case here. It is expected that the relative error will be largest when the modeled system is in an equilibrium state, such as occurs during long-term simulations, and will be less noticable on an event scale.

Errors due to time averaging are by far the most significant during and shortly after rainfall events. It was demonstrated that almost all of the difference between a time-averaged simulation and one which is not averaged arises from averaging within the vicinity of the precipitation events. During the precipitation events, it is most important to capture the variability of the precipitation rate: the next most important weather component is the atmospheric vapor density. Nevertheless, ignoring variability in any of the atmospheric components can result in significant errors. The implication is that a storm characterized by trace rainfall over several hours with one or more intense bursts of rain may yield significantly more infiltration than a storm that has the same cumulative amount of rainfall uniformly spread over the same length of time.

Simulation results are remarkably insensitive to the characterization of the atmosphere during the soil-controlled interstorm intervals. Atmospheric conditions only affect the soil moisture profile directly when the ground surface is moist: once the top few centimeters have dried sufficiently to limit evaporation to the amount of moisture that vapor transport can yield, flow in the porous media is effectively decoupled from atmospheric perturbations. For the two arid environments considered, the dryout time appears to be less than two days for almost every storm.

When comparing the simulation times using the raw input data and using monthly averaged weather, simulations using averaging were up to four times faster than simulations using the raw data. In the averaging simulations, averaged inputs were provided on an hourly basis; however, convergence in the inter-storm periods was very fast. Although simply using an event window of hourly readings around each precipitation event while using long-term averaged data elsewhere is shown to be an effective way to use long-term averaged input without sacrificing accuracy, it is unlikely that such a strategy could perform much faster than the corresponding case with monthly averaged parameters.

Using reasonable ranges for alluvium parameters, the behavior of long-term simulations was examined by cycling a ten-year hourly weather sequence repeatedly until a cyclic steady state was achieved. The considered range in K_{sat} spanned three orders of magnitude; net deep infiltration also spanned nearly three orders of magnitude. However, surprisingly the net deep infiltration varied inversely with K_{sat}. One implication of this result is that K_{sat} may be quite misleading as an indicator of actual infiltration into a porous continuum.

The work reported in this paper is one step in ongoing projects aimed at improving representation of deep infiltration fluxes at Yucca Mountain. The simulator is intended to be used in further work characterizing infiltration fluxes in several ways: (i) linked with a GIS database describing Yucca Mountain and a synthetic weather generator, estimating spatial variability of shallow infiltration fluxes; (ii) providing top boundary conditions for a model characterizing deep moisture flow; and (iii) as a comparison tool for simpler models. An important goal of the work is to improve the representation of moisture movement within performance assessment models of Yucca Mountain, as infiltration fluxes are found to be arguably the most important determinant of repository performance.

This paper was prepared to document work performed by the Center for Nuclear Waste Regulatory Analyses (CNWRA) for the NRC under Contract No. NRC-02-93-005. The activities reported here were performed on behalf of the NRC Office of Nuclear Material Safety and Safeguards, Division of Waste Management. The report is an independent product of the CNWRA and does not necessarily reflect the views or regulatory position of the NRC. The version of the BREATH code

used in this report is not controlled under the CNWRA's Software Configuration Procedure.

The author would like to acknowledge the technical reviews by R.G. Baca and A.C. Bagtzoglou which greatly improved this paper.

APPENDIX: BOUNDARY CONDITIONS

Ground surface albedo (α_s) and emissivity (ϵ_s) are assumed to be simple linear functions of saturation:

$$\alpha_s = \alpha_s^{dry} + \theta_{eff}(\alpha_s^{dry} - \alpha_s^{wet}), \tag{22}$$

$$\epsilon_s = \epsilon_s^{dry} + \theta_{eff}(\epsilon_s^{dry} - \epsilon_s^{wet}), \tag{23}$$

$$\theta_{eff} = (\theta_w - \theta_{wr})/(\theta_{ws} - \theta_{wr}), \tag{24}$$

where the *wet* and *dry* superscripts refer to the values at full saturation and residual saturation.

Boundary conditions for both the moisture and the energy balance equations require estimation of the boundary layer conductance. Calculation of the boundary layer conductances is based on a linearized form of relationships found in Campbell (1985) and Brutsaert (1982):

$$k_v(V) = \begin{cases} \max(a + bV, D_{va}/z), & \text{if } V < V_1 \\ k_{bl} & \text{if } V \geq V_1 \end{cases} \tag{25}$$

$$k_h(V) = \rho_a C_P k_v, \tag{26}$$

$$a = (1/2)[k_{bl}(V_1) + k_{bl}(V_2) - b(V_1 + V_2)] \tag{27}$$

$$b = [k_{bl}(V_2) - k_{bl}(V_1)]/(V_2 - V_1) \tag{28}$$

$$k_{bl}(V) = \kappa U/(\ln[(z + z_h)/z_h] - \Psi_h), \tag{29}$$

$$U = \kappa V/(\ln[(z + z_m)/z_m] - \Psi_m), \tag{30}$$

$$\zeta = -\kappa g(z + z_m)[H/(T_a C_P) + 0.61E]/\rho_a U^3, \tag{31}$$

$$H = \rho_a C_P k_{bl}(T - T_a), \tag{32}$$

$$E = k_{bl}(\rho_v - \rho_{va}), \tag{33}$$

$$\Psi_m = \begin{cases} -5[1 + \ln(\zeta)] & \text{if } 1 < \zeta, \\ -5\zeta & \text{if } 0 \leq \zeta \leq 1, \\ 2\ln[(1 + x)/2] + \ln[(1 + x^2)/2] - 2\arctan(x) + \pi/2 & \text{if } \zeta < 0. \end{cases} \tag{34}$$

$$\Psi_h = \begin{cases} \Psi_m & \text{if } \zeta \geq 0. \\ 2\ln[(1 + x^2)/2] & \text{if } \zeta < 0. \end{cases} \tag{35}$$

$$x = (1 - 16\zeta)^{1/4}, \tag{36}$$

where V is the wind speed, V_1 and V_2 are arbitrary large wind speeds ($V_1 < V_2$), κ is the von Karman constant, D_{va} is the diffusion coefficient for vapor in air, z is the measurement height for atmospheric properties, z_m and z_h are the roughness height for momentum and heat, and T and T_a are soil and atmospheric temperatures.

References

Black, T. A., W. R. Gardner, and G. W. Thurtell. 1969. The prediction of evaporation, drainage, and soil water storage for a bare soil. Soil Science Society of America Journal v. 33, no. 5, pp. 655–660.

Brutsaert, W. 1982. Evaporation into the Atmosphere: Theory, History, and Applications. Dordrecht, The Netherlands: Kluwer Academic Publishers.

Campbell, G. S. 1985. Soil Physics with BASIC. Amsterdam, The Netherlands: Elsevier Science Publishers B.V.

Celia, M. A., E. T. Bouloutas, and R. L. Zarba. 1990. A general mass-conservative numerical solution for the unsaturated flow equation. Water Resources Research v. 26, no. 7, pp. 1483–1496.

Clapp, R. B. 1982. A wetting front model of soil water dynamics. Ph. D. thesis, University of Virginia, Charlottesville, VA.

Czarnecki, J. B. 1990. Geohydrology and evapotranspiration at Franklin Lake Playa, Inyo County, California. Open-File Report 90-356, United States Geological Survey, Denver, CO.

Eagleson, P. S. 1978. Climate, soil, and vegetation: 3. A simplified model of soil moisture movement in the liquid phase. Water Resources Research v. 14, no. 5, pp. 722–730.

Electric Power Research Institute. 1990. Demonstration of a risk-based approach to high-level waste repository evaluation. EPRI NP-7057, Electric Power Research Institute, Palo Alto, CA.

Electric Power Research Institute. 1992. Demonstration of a risk-based approach to high-level waste repository evaluation: Phase 2. EPRI TR-100384, Electric Power Research Institute, Palo Alto, CA.

Flint, A. L. and L. E. Flint. 1994. Spatial distribution of potential near surface moisture flux at Yucca Mountain. In *Proceedings of the Fifth Annual High Level Radioactive Waste Management Conference*, La Grange Park, IL, pp. 2352–2358. American Nuclear Society.

Gardner, H. R. 1973. Prediction of evaporation from homogeneous soil based on the flow equation. Soil Science Society of America Journal v. 37, no. 4, pp. 513–516.

Gardner, H. R. 1974. Prediction of water loss from a fallow field soil based on soil water flow theory. Soil Science Society of America Journal v. 38, no. 3, pp. 379–382.

Guertal, W. R., A. L. Flint, L. L. Hofmann, and D. B. Hudson. 1994. Characterization of a desert soil sequence at Yucca Mountain, NV. In *Proceedings of the Fifth Annual High Level Radioactive Waste Management Conference*, La Grange Park, IL, pp. 2755–2763. American Nuclear Society.

Hevesi, J. A. and A. L. Flint. 1993. The influence of seasonal climatic variability on shallow infiltration at Yucca Mountain. In *Proceedings of the Fourth Annual High Level Radioactive Waste Management Conference*, La Grange Park, IL, pp. 122–131. American Nuclear Society.

Hevesi, J. A., A. L. Flint, and L. E. Flint. 1994. Verification of a 1-dimensional model for predicting shallow infiltration at Yucca Mountain. In *Proceedings of the Fifth Annual High Level Radioactive Waste Management Conference*, La Grange Park, IL, pp. 2323–2332. American Nuclear Society.

Hudson, D. B., A. L. Flint, and W. R. Guertal. 1994. Modeling a ponded infiltration experiment at Yucca Mountain, NV. In *Proceedings of the Fifth Annual High Level Radioactive Waste Management Conference*, La Grange Park, IL, pp. 2168–2174. American Nuclear Society.

McKinley, P. and T. Oliver. 1994. Meteorological, stream-discharge, and water-quality data for 1986 through 1991 from two small basins in central Nevada. Open-File Report 93-651, United States Geological Survey, Denver, CO.

Milly, P. C. D. 1984a. A linear analysis of thermal effects on evaporation from soil. Water Resources Research v. 20, no. 8, pp. 1075–1085.

Milly, P. C. D. 1984b. A simulation analysis of thermal effects on evaporation from soil. Water Resources Research v. 20, no. 8, pp. 1087–1098.

Milly, P. C. D. 1986. An event-based simulation model of moisture and energy fluxes at a bare soil surface. Water Resources Research v. 22, no. 12, pp. 1680–1692.

Mualem, Y. 1976. A new model for predicting the hydraulic conductivity of unsaturated porous media. Water Resources Research v. 12, no. 3, pp. 513–522.

Nuclear Regulatory Commission. 1992. Initial demonstration of the NRC's capability to conduct a performance assessment for a high-level waste repository. NUREG-1327, Nuclear Regulatory Commission, Washington, DC.

Nuclear Regulatory Commission. 1994. Phase 2 demonstration of the NRC's capability to conduct a performance assessment for a high-level waste repository. NUREG-1464, Nuclear Regulatory Commission, Washington, DC. In press.

Paniconi, C., A. A. Aldama, and E. F. Wood. 1991. Numerical evaluation of iterative and non-iterative methods for the solution of the nonlinear Richards equation. Water Resources Research v. 27, no. 6, pp. 1147–1163.

Salvucci, G. 1994. Hillslope and climatic controls on hydrologic fluxes. Ph. D. thesis, Massachusetts Institute of Technology, Cambridge, MA.

Sandia National Laboratories. 1992. TSPA 1991: An initial total-system performance assessment for Yucca Mountain. SAND91-2795, Sandia National Laboratories, Albuquerque, NM.

Sandia National Laboratories. 1994. Total-system performance assessment for Yucca Mountain–SNL second iteration (TSPA-1993). SAND93-2675, Sandia National Laboratories, Albuquerque, NM.

Stothoff, S. 1995. BREATH version 1.1–Coupled flow and energy transport in porous media: Simulator description and user guide. NUREG-CR 94-020, Nuclear Regulatory Commission, Washington, DC.

van Genuchten, M. T. 1980. A closed-form equation for predicting the hydraulic conductivity of unsaturated soils. Soil Science Society of America Journal v. 44, pp. 892–898.

Young, D. R. and P. S. Nobel. 1986. Predictions of soil-water potentials in the north-western Sonoran desert. Journal of Ecology v. 74, pp. 143–154.

Table 1: Material properties used for Figure 4.

Material	K_{sat} m/s	α 1/m	n	ε	θ_w
synth	1×10^{-6}	0.1	1.3	0.098	0.0247
PTn	5.2×10^{-7}	1.37	1.48	0.403	0.14
TCmw	3.9×10^{-9}	0.237	2.2	0.24	0.07
TCw	2.7×10^{-11}	0.065	1.38	0.078	0.06

Table 2: Storm cutoff sizes and corresponding storm percentages.

Cutoff Event (in/hr)	Total Events	Percent
1	3	0.17
0.3	14	0.82
0.1	114	6.6
0.03	678	39.5
0.01	1208	70.4

Table 3: Material properties used for Figure 5.

K_{sat} m/s	α 1/Pa$\times10^4$	m	$\overline{\theta_w}$	$\overline{q_m}$ cm/yr
10^{-6}	5	0.1	0.206	0.145
10^{-6}	5	0.2	0.147	0.69
10^{-6}	5	0.3	0.114	2.9
10^{-3}	10	0.2	0.06	0.055
10^{-4}	10	0.2	0.083	0.18
10^{-5}	10	0.2	0.126	1.42
10^{-6}	10	0.2	0.166	2.58
10^{-6}	2	0.2	0.117	0.065
10^{-3}	2	0.2	0.047	0.0042

Figure 1: Result of averaging all weather inputs. (a) Ten-year-average moisture content profile. (b) Ten-year-average moisture flux profile.

Figure 2: Effect of varying individual parameters over their range.

Figure 3: Effect of using a single raw weather input within a two-day event window with all other variables averaged.

Figure 4: Effect of considering various material properties.

Figure 5: Sensitivity of long-term moisture content and moisture flux to K_{sat} and van Genuchten α and m.

Figure 1a

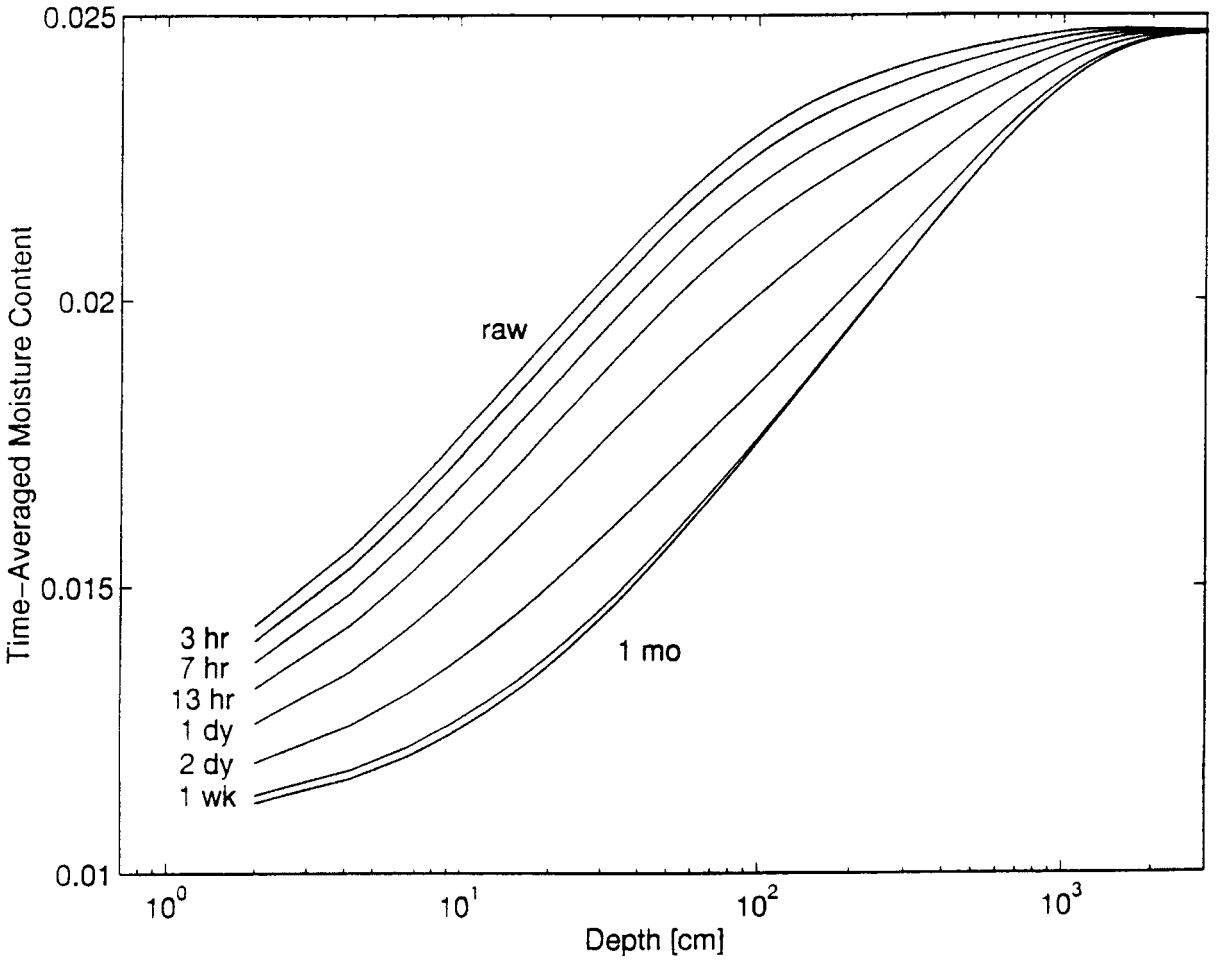
0.025
0.02
0.015
0.01
Time-Averaged Moisture Content
raw
3 hr
7 hr
13 hr
1 dy
2 dy
1 wk
1 mo
10^0
10^1
10^2
10^3
Depth [cm]

Figure 1b

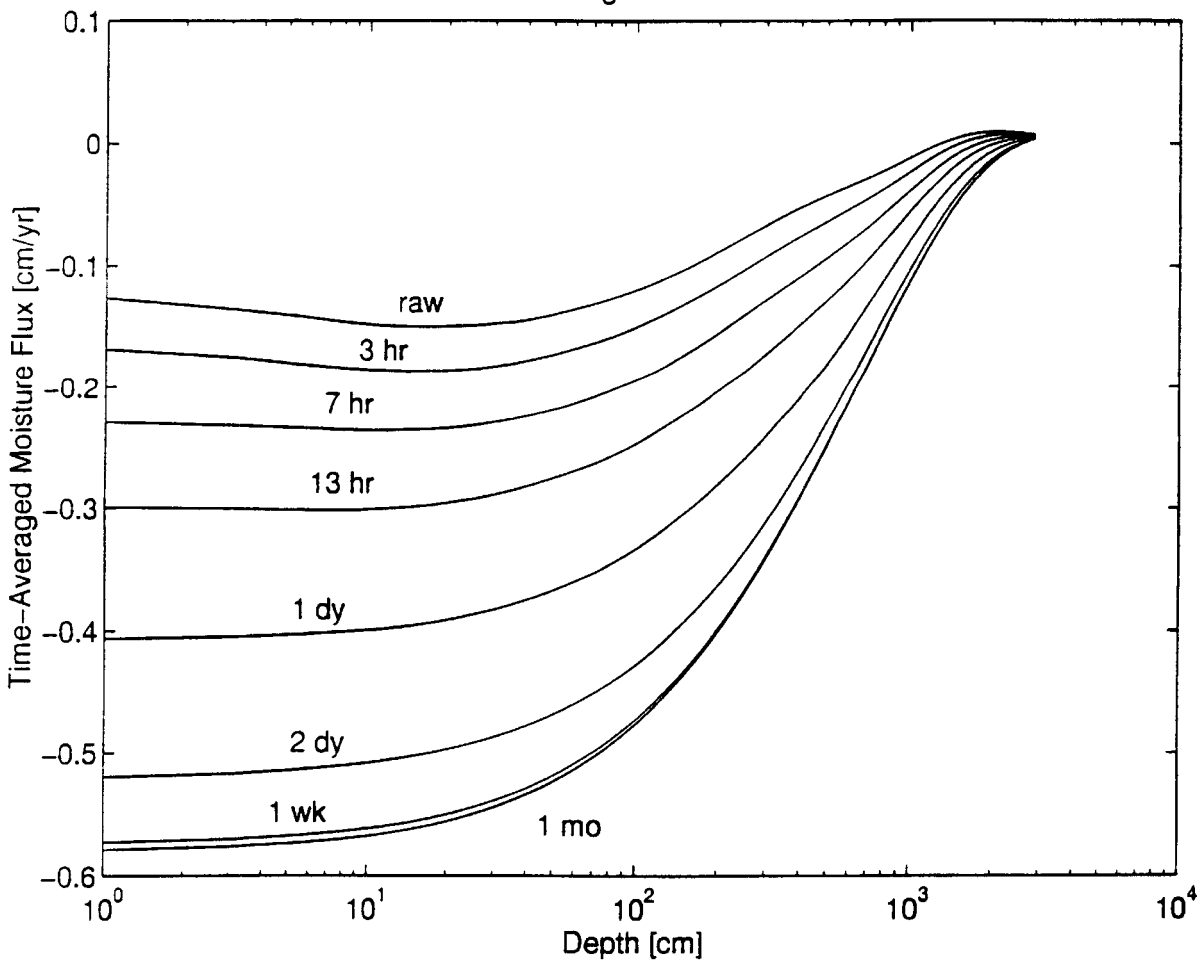
0.1
0
−0.1
−0.2
−0.3
−0.4
−0.5
−0.6
Time−Averaged Moisture Flux [cm/yr]
raw
3 hr
7 hr
13 hr
1 dy
2 dy
1 wk
1 mo
10^0
10^1
10^2
10^3
10^4
Depth [cm]

Figure 2

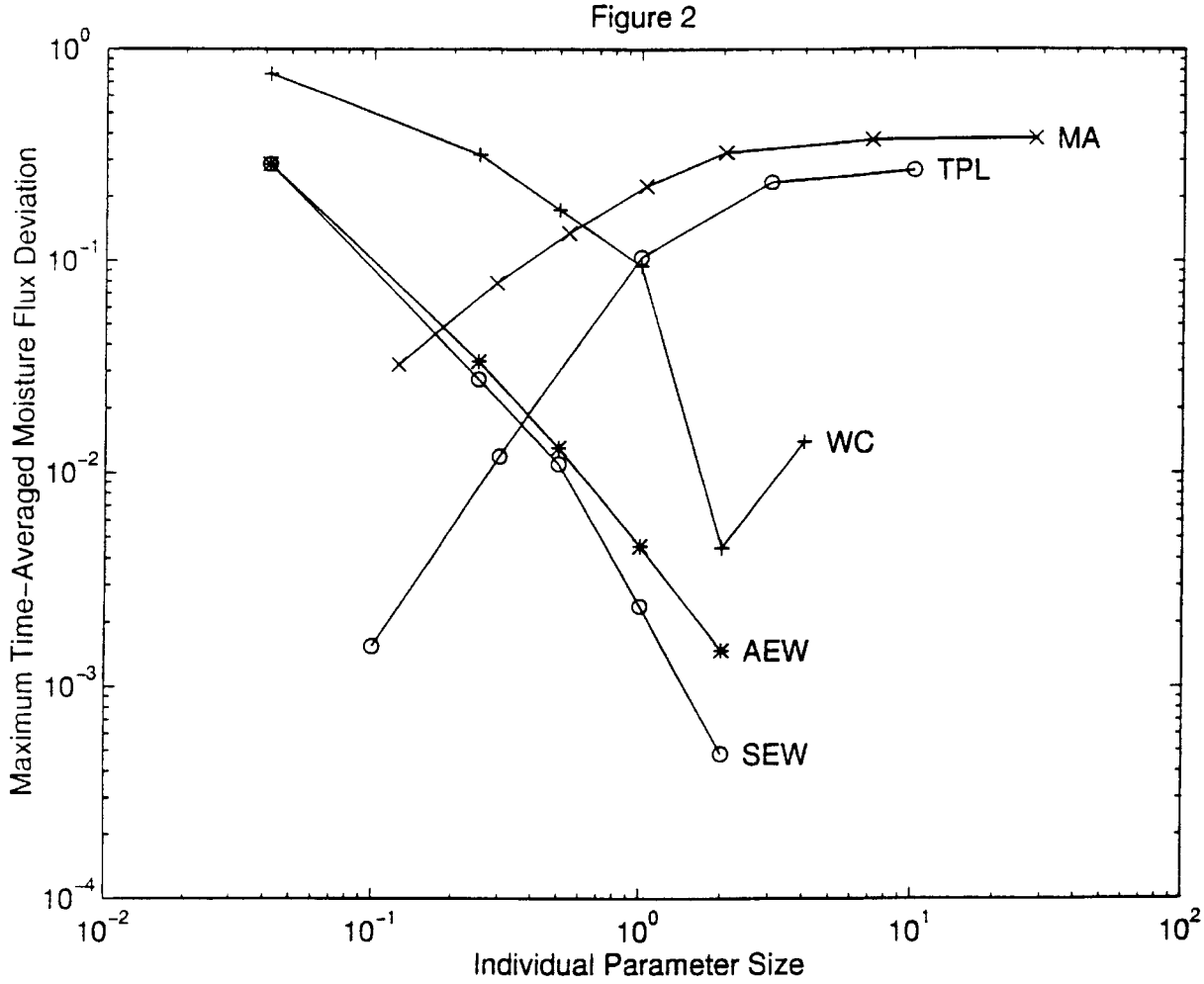
Maximum Time-Averaged Moisture Flux Deviation
Individual Parameter Size
MA
TPL
WC
AEW
SEW

Figure 3

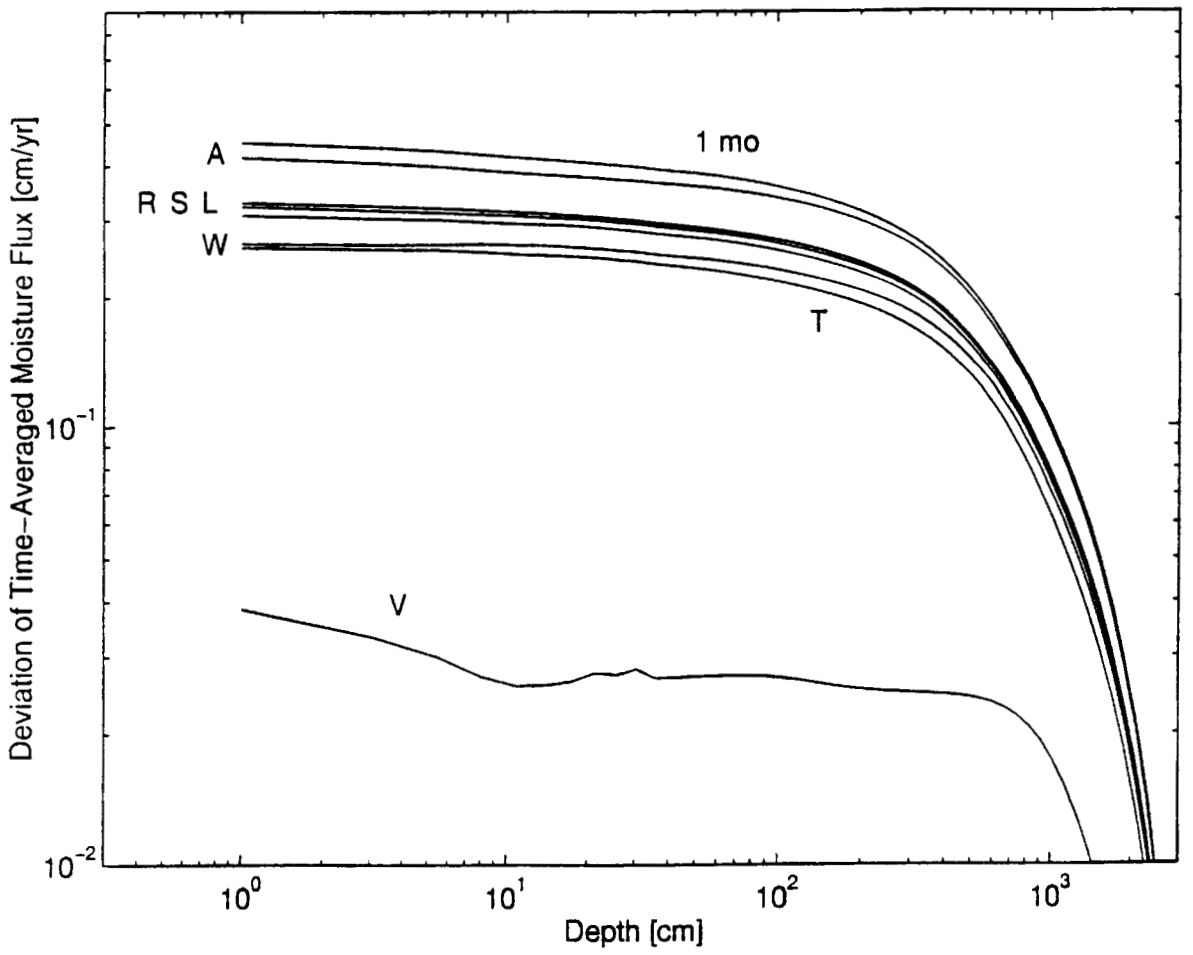
Deviation of Time-Averaged Moisture Flux [cm/yr]
10^{-1}
10^{-2}
A
R S L
W
1 mo
T
V
10^0
10^1
10^2
10^3
Depth [cm]

Figure 4

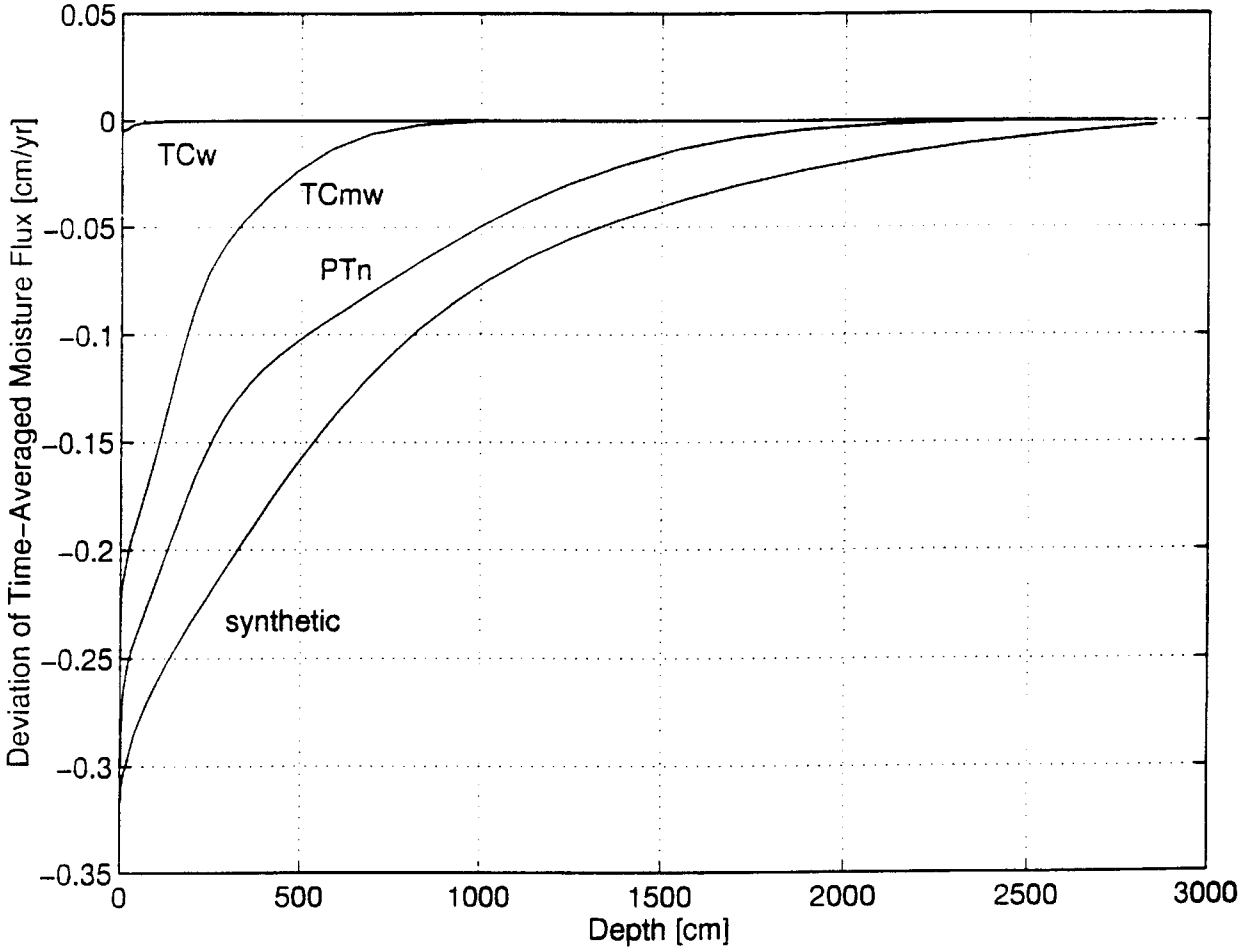
0.05
0
−0.05
−0.1
−0.15
−0.2
−0.25
−0.3
−0.35
0
500
1000
1500
2000
2500
3000
Deviation of Time−Averaged Moisture Flux [cm/yr]
Depth [cm]
TCw
TCmw
PTn
synthetic

Figure 5

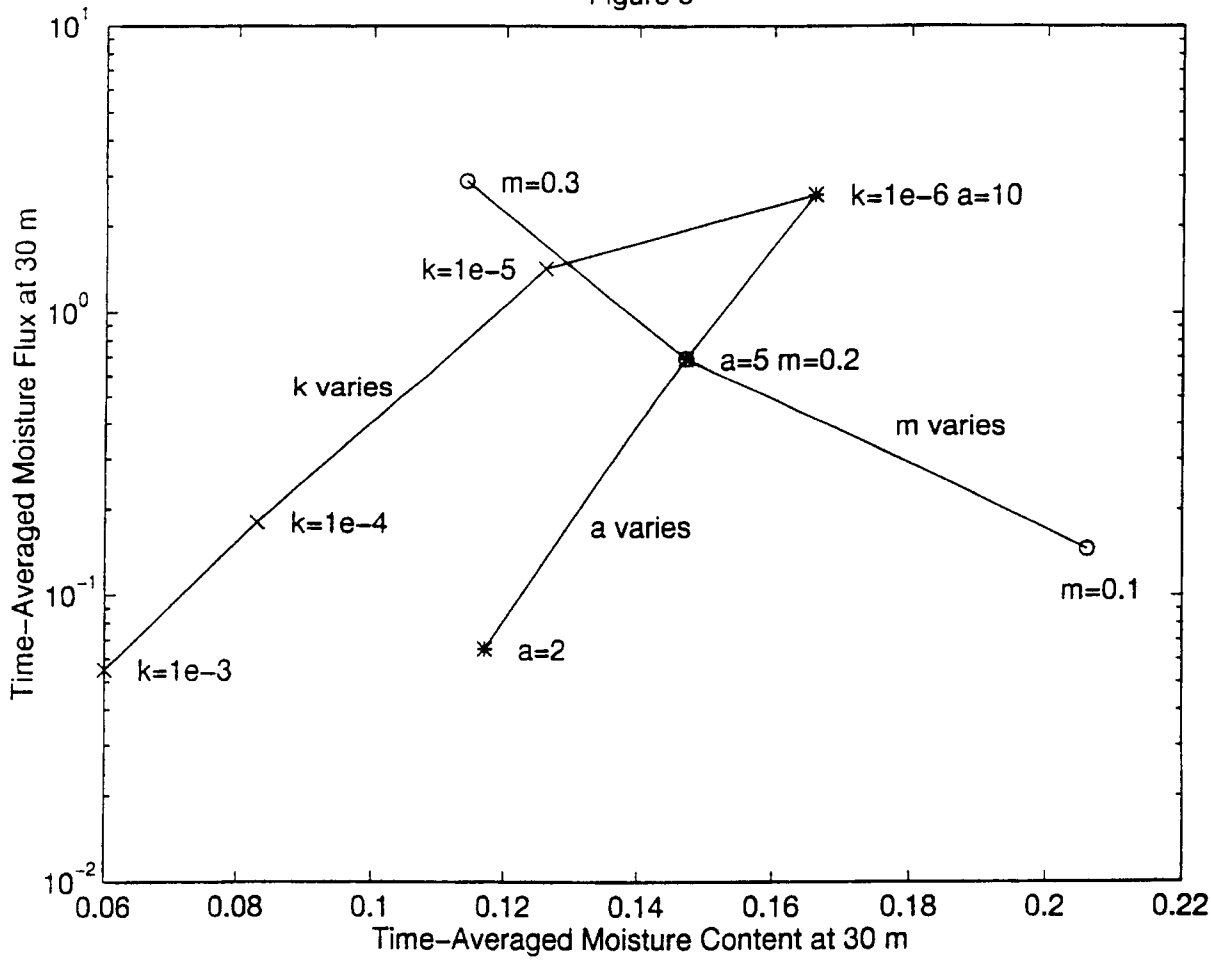
10^1
10^0
10^{-1}
10^{-2}
Time–Averaged Moisture Flux at 30 m
0.06
0.08
0.1
0.12
0.14
0.16
0.18
0.2
0.22
Time–Averaged Moisture Content at 30 m
m=0.3
k=1e–6 a=10
k=1e–5
a=5 m=0.2
k varies
m varies
k=1e–4
a varies
m=0.1
a=2
k=1e–3